PCCP

PAPER

View Article Online
View Journal

Cite this: DOI: 10.1039/c9cp01049a

Single-particle correlation study: chemical interface damping induced by biotinylated proteins with sulfur in plasmonic gold nanorods†

Seong Woo Moon and Ji Won Ha *

Received 22nd February 2019,
Accepted 11th March 2019

DOI: 10.1039/c9cp01049a

rsc.li/pccp

Plasmonic gold nanoparticles can be an efficient source of hot electrons that can transfer to adsorbed molecules for photochemistry, followed by broadening of the homogeneous localized surface plasmon resonance (LSPR) linewidth. Although chemical interface damping (CID) is one of the main decay processes, it is the most poorly understood damping mechanism in gold nanoparticles. Herein, to better understand CID and to find new functional groups that can induce CID as an alternative to thiol groups (–SH, sulfhydryl groups), we carried out scanning electron microscopy (SEM) correlated dark-field (DF) scattering studies of gold nanorods (AuNRs) at the single-particle level. We found that biotin with sulfur can lead to strong plasmon damping in single AuNRs. We chose biotin in this study because it is widely used as a linker that can selectively bind to streptavidin in many biological sensing experiments. We further demonstrated the possibility of real-time detection of biological molecules, specifically biotinylated BSA proteins, by means of CID in single AuNRs. Therefore, this study allows us to gain a deeper insight into how adsorbate molecules with sulfur affect CID, which is an important step toward developing a CID-based LSPR biosensor to detect real biological molecules having sulfur or thiol groups without interference from the medium dielectric constant in single AuNRs.

Introduction

Plasmon relaxation pathways in gold nanoparticles are gaining much interest because of their potential applications in a variety of photochemical reactions, photocatalysis, and bio-sensing experiments. To date, the plasmon relaxation pathways have been mainly investigated by means of ultrafast spectroscopy techniques on the smallest timescale. However, such ultrafast spectroscopic techniques have disadvantages such as high cost and inconvenience of processing.[1] As an alternative, homogeneous localized surface plasmon resonance (LSPR) linewidth measurements, using only single nanoparticles over the heterogeneous linewidth of an ensemble spectrum, allowed for overcoming the timescale limitation.[2–4] Because of the proportional relationship between the LSPR linewidth and the plasmon damping rate, the homogeneous LSPR linewidth, using far-field single-particle spectroscopy techniques, can be effectively used to investigate the total plasmon damping pathways.[5]

Recently, several groups have employed scattering-based dark-field (DF) microscopy and spectroscopy to examine the LSPR linewidth broadening of single gold nanoparticles.[4,6–10] The homogeneous LSPR linewidth is affected by lifetime broadening caused by various plasmon damping pathways, including bulk metal damping Γ_{bulk}, electron-surface scattering Γ_{surf}, radiation damping Γ_{rad}, and chemical interface damping (CID) Γ_{CID}.[3,7,10–15] Therefore, the following eqn (1) describes the total LSPR damping channel:

$$\Gamma_{tot} = \Gamma_{bulk} + \Gamma_{rad} + \Gamma_{surf} + \Gamma_{CID} \quad (1)$$

Among the plasmon damping processes, CID is the most recently proposed plasmon decay pathway. Recent findings on interfacial hot-electron transfer have shown that two decay pathways can be followed in metal/adsorbate interfacial systems, depending on the way that the adsorbate molecules are bound onto the metal. The first pathway is the conventionally known indirect transfer, and the second is the recently reported direct transfer, noted above as CID.[15,16] In the former pathway, after hot electrons are generated, they are transferred to empty orbitals (LUMOs: lowest unoccupied molecular orbitals) of the adsorbates (Scheme 1A).[17–19] In the latter pathway, a strong interaction between the adsorbates and metal at their interface induces an additional dephasing channel (or CID), which result in the direct generation of hot electrons for the available LUMO acceptors of the adsorbate (Scheme 1B).

So far, there have been few studies to reveal the chemical effect on plasmon damping at the single-particle level, and

Advanced Nano-Bio-Imaging and Spectroscopy Laboratory, Department of Chemistry, University of Ulsan, 93 Daehak-ro, Nam-gu, Ulsan 44610, Republic of Korea. E-mail: jwha77@ulsan.ac.kr; Fax: +82 52 712 8002; Tel: +82 52 712 8012

† Electronic supplementary information (ESI) available: Additional experimental details and results. See DOI: 10.1039/c9cp01049a

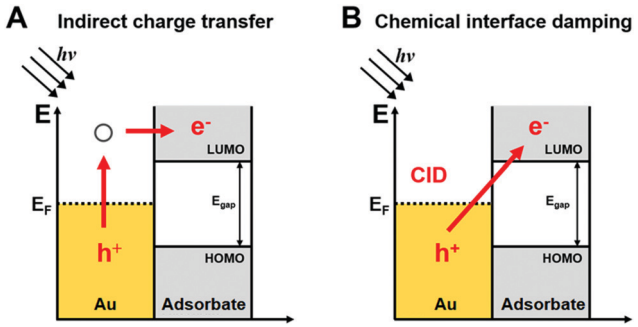

Scheme 1 Schematics to depict the two mechanisms for hot-electron transfer generated in gold to adsorbate molecules. (A) Indirect mechanism to show the generation of hot electrons before they are transferred to LUMOs. (B) Direct mechanism (or chemical interface damping) to show the generation of hot electrons directly in LUMOs.

recent studies have used the homogeneous LSPR linewidth of single gold nanorods (AuNRs). For instance, size-dependent broadening of the homogeneous LSPR linewidth was demonstrated by altering the chemical environment of single AuNRs with a similar aspect ratio (AR).[14] CID has been found to depend on hot electrons reaching the surface, confirmed by the time evolution of the Langmuir adsorption model in surface chemistry. Very recently, single-particle DF scattering studies have been reported to deepen our understanding of the CID effect in single AuNRs with different ARs.[13,20]

Although there have been recent studies on CID using single-particle spectroscopy, our understanding of CID is still very limited in two important ways.[14] First, recent studies on CID were based on thiol molecules, which have a strong binding affinity for gold. However, the effect on CID of using adsorbate molecules with different functional groups is largely unknown. Second, recent studies showed that CID, rather than the LSPR frequency shift, can be used as an alternative for developing biosensors without interference from the medium dielectric constant.[13] However, it has not been demonstrated that CID can be used to detect real biological molecules in the development of biosensors with high sensitivity and selectivity. In this respect, it is highly desirable to address the aforementioned two ways by carrying out single-particle DF studies with single AuNRs.

In this study, SEM-correlated DF scattering studies of single AuNRs were performed to elucidate the CID phenomenon at the single-particle level. Particularly, we tried to find other adsorbate molecules, besides the thiol group, that can induce LSPR linewidth broadening in single AuNRs. Biotin can lead to strong plasmon damping in single AuNRs through specific Au–sulfur interactions. We chose biotin in this study because it is widely used as a linker specifically bound to streptavidin in many biological sensing experiments. Finally, we checked the possibility of using the CID of single AuNRs for real-time detection of actual biological molecules, specifically, biotinylated BSA proteins.

Experimental section

Materials

Bovine serum albumin (BSA) and biotin were purchased from Sigma Aldrich (St. Louis, MO, USA). Biotinylated BSA was obtained from Thermo Fisher (Waltham, MA, USA). Citrate-stabilized AuNRs (25 nm × 73 nm) were purchased from Nanopartz (Loveland, CO, USA).

Sample preparation and characterization

Microscope cover glasses were cleaned by sonicating in methanol for 10 min, followed by acetone for 10 min. The solution containing AuNRs was diluted to a proper concentration and sonicated for 10 min to prevent the aggregation of the AuNRs. A sample was prepared by drop casting the diluted AuNR solution onto patterned and aminosilanized glass slides. In this study, citrate-stabilized AuNRs were immobilized on the glass slides by a silane method with APTES. We adjusted the concentration of AuNRs fixed on the glass surface to be about 1 μm^{-2} for single AuNR characterization without interparticle LSPR coupling. Characterization was performed using a FEI Quanta ESEM2 SEM operated under a low vacuum in a water-vapor atmosphere at 30 kV.

Single-particle scattering microscopy and spectroscopy

In this study, we performed a correlation study between SEM and DF microscopy for the same AuNRs. DF scattering images were collected on a home-built microscope by using an inverted Nikon microscope with a tungsten lamp. We used electronic control of the sample stage to achieve an X–Y resolution of a hundred nanometers in our system. We acquired scattering spectra of single AuNRs with a spectrometer (Andor, SHAMROCK 303i, SR-303I-A) and a CCD camera (Andor, Newton DU920P-OE). When taking a spectrum, we used the scanning stage to move the sample to the desired location; thus, only the scattered light from the selected location was sent to the Andor spectrometer, dispersed by a grating (300 l mm^{-1}), and detected by the Newton CCD camera. We obtained the background spectrum at a region having no Au particles. We carried out data analysis by using specially designed Matlab programs. Finally, we fitted the experimental spectra with a Lorentzian function, $I(\omega) = C_0/[(\omega - \omega_0)^2 + \Gamma^2/4]$, to yield the LSPR linewidth Γ and the LSPR wavelength ω_0.

Correlation study

In this study, the obtained SEM images were correlated with DF scattering images and spectra of single AuNRs. After cleaning the glass slides, we created a gold pattern by evaporating a 5 nm Ti layer and then a 20 nm Au layer through an indexed copper Transmission Electron Microscopy (TEM) grid (Ted Pella) placed on the cleaned glasses. First, we took SEM images of single AuNRs that were well separated on a glass slide. We then obtained DF scattering images of the same AuNRs under optical microscopy. Therefore, the Au pattern enabled us to locate the same AuNRs in SEM and DF scattering microscopy.

Results and discussion

We first measured the size of AuNRs by scanning electron microscopy (SEM), and their average length and width were calculated to be 72.3 (±9.01) nm and 22.3 (±2.17) nm,

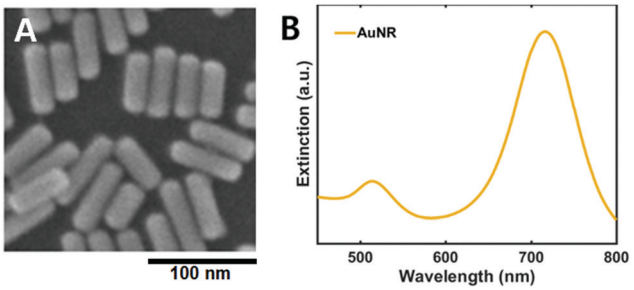

Fig. 1 (A) SEM image of single AuNRs having an AR of 3.24 (72.3 nm × 22.3 nm). (B) UV-vis extinction spectrum of AuNRs in pure water.

respectively (Fig. S1, ESI†). Fig. 1A shows an SEM image of AuNRs with anisotropic shape, and their extinction spectrum in distilled water was obtained by a Varian Cary 300 UV-vis spectrophotometer (Fig. 1B). For anisotropic AuNRs, two characteristic transverse and longitudinal peaks are observed. The transverse LSPR peak was observed at approximately 514 nm, whereas the longitudinal LSPR peak was seen at 706 nm for the AuNRs (72.3 nm × 22.3 nm) measured in this study, which is consistent with previous studies.[13,20] However, the ensemble measurement is limited by the heterogeneity issue (size and shape); thus, a single-particle study is desirable to reveal size- and shape-dependent unique optical properties of AuNRs without ensemble averaging.

In this study, we performed SEM-correlated dark-field (DF) scattering measurements of AuNRs at the single-particle level. When a solution containing AuNRs was drop cast on a glass slide, citrate-stabilized AuNRs were immobilized on the aminosilanized glass slide. A photograph showing the experimental setup for DF scattering microscopy and spectroscopy is provided in Fig. S2 (ESI†). As shown in Fig. S3 (ESI†), DF microscopy is based on the scattering of AuNRs that have large scattering and absorption cross-sections, and scattered light from the sample is collected by the numerical aperture (NA) adjustable objective lens, avoiding interference from the excitation lamp. We employed SEM to obtain detailed information on the size and shape of AuNRs, and their SEM images were then correlated with DF scattering images and scattering spectra of single AuNRs.[13] By using correlated SEM and optical imaging, we ensured that single particles were measured within the diffraction-limited optical detection area. We describe the experimental methods used in the correlation study in detail in the ESI.†

Fig. 2A shows a DF scattering image of single AuNRs with an AR of 3.24 (72.3 nm × 22.3 nm on average), and Fig. 2B shows a correlated SEM image for the same AuNRs. Afterwards, the scattering spectra of single AuNRs were obtained to characterize their scattering properties. Fig. 2C shows the scattering spectra of three AuNRs highlighted by a square in Fig. 2A. We observed that the scattering spectra of single AuNRs show a LSPR peak at around 715 nm, corresponding to longitudinal surface plasmon resonance. Furthermore, the single particle spectrum is consistent with the ensemble spectrum presented in Fig. 1B.

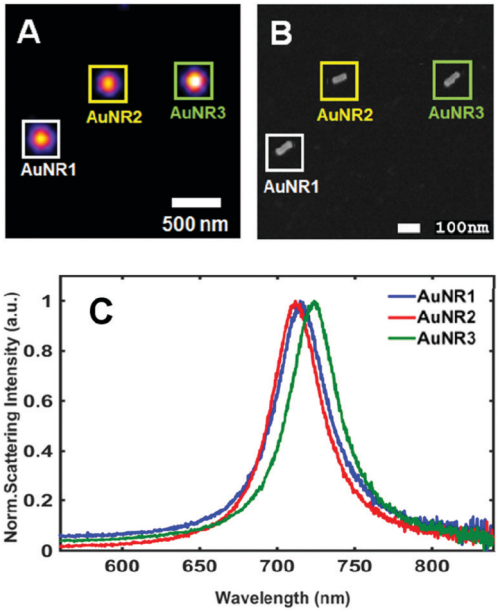

Fig. 2 (A) Dark-field scattering image of single AuNRs. (B) Correlated SEM image of the same AuNRs as in (A). (C) Single-particle scattering spectra of the three AuNRs highlighted with a square in (A).

LSPR linewidth broadening is closely associated with the reduction of the lifetime of the surface plasmon excitation. So far, the CID effect of AuNRs has been studied using thiol molecules, because the thiol group (–SH) has a strong binding affinity for gold. However, the effect on CID of using adsorbate molecules with other functional groups is largely unknown. Furthermore, CID has not been studied with real biological molecules in trying to develop CID-based biosensors. In this regard, we tried to address the aforementioned two aspects by carrying out single-particle DF measurements with single AuNRs and biotinylated BSA proteins (Fig. 3A). We chose biotin in this study because it contains a sulfur group that can bond with the Au surfaces, as depicted in Fig. 3B. We therefore checked if biotin's sulfur group can induce the CID effect by adsorbing on the AuNR surfaces.

First, we used DF microscopy and spectroscopy to investigate the LSPR linewidth broadening caused by chemical

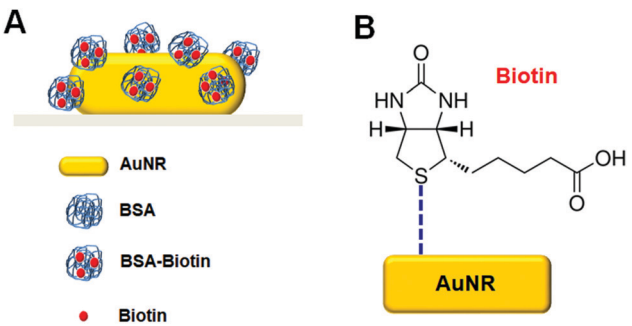

Fig. 3 (A) Schematic of a single AuNR interacting with BSA-biotin. (B) Schematic to show the chemical bond of the sulfur in biotin with the AuNR surface.

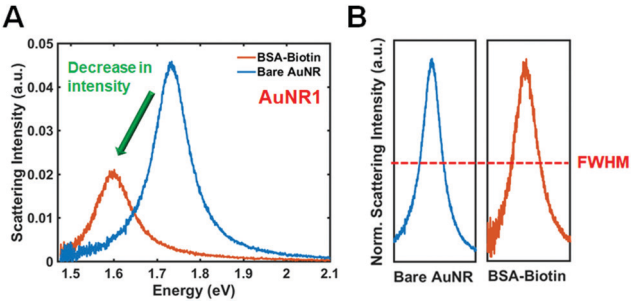

Fig. 4 (A) Single particle scattering spectra of AuNR1 in water (blue) and after adding BSA-biotin in water (red). The scattering spectra are presented in eV. (B) The change in the LSPR linewidth is better illustrated when the two spectra are normalized.

interactions of biotinylated BSA with single AuNR particles. Fig. 4A shows single-particle scattering spectra of AuNR1 in water (blue curve) and after adding BSA-biotin in water (red curve). Interestingly, the BSA-biotin caused both a red shift and strong plasmon damping with a much reduced scattering intensity and broadening of the linewidth. The decrease of the scattering intensity induced by the biotin adsorption was further confirmed by a statistical analysis in Fig. S4 (ESI†). The LSPR linewidth broadening is better illustrated with the same spectra normalized as shown in Fig. 4B. The full width at half maximum (FWHM) values were calculated to be 102 meV and 117 meV for the blue and red spectra, respectively, by Lorentzian fitting. As shown in Fig. S5 (ESI†), the experimental data were fit well with the Lorentzian function. Therefore, the increase in the LSPR linewidth can be ascribed to strong chemical interactions between the adsorbed thiol molecules and the AuNR surfaces. Therefore, we have provided a deeper insight into how the LSPR linewidth of single AuNRs is influenced by chemical adsorption of biotinylated BSA onto the particle surface by the Au–sulfur interaction.

Second, we further conducted a control experiment with BSA under the same experimental conditions. In this control experiment, we tried to confirm that biotin conjugated on BSA induces LSPR broadening by means of the Au–sulfur interaction on the particle surface. As seen in Fig. 5A, the LSPR wavelength was red-shifted because of the change in the surrounding refractive index by the adsorption of BSA molecules on the NR surface more than was that of bare AuNRs. However, it is notable that the LSPR linewidth (or FWHM) in the presence of BSA remained almost the same as that of bare AuNRs (Fig. 5B). The results support that BSA molecules do not cause the CID phenomenon that results in the LSPR broadening and that the LSPR broadening from BSA-biotin (Fig. 4 and 5) is induced by biotin conjugated on BSA. To verify the effect of biotin on CID more clearly, we carried out another control experiment with biotin only under the same experimental conditions. The LSPR wavelength was shifted to a longer wavelength by the adsorption of biotin molecules on the NR surface *via* the Au–sulfur interaction (Fig. 5A). Furthermore, as compared to bare AuNRs, the LSPR linewidth in the presence of biotin was increased up to 113 meV, which is

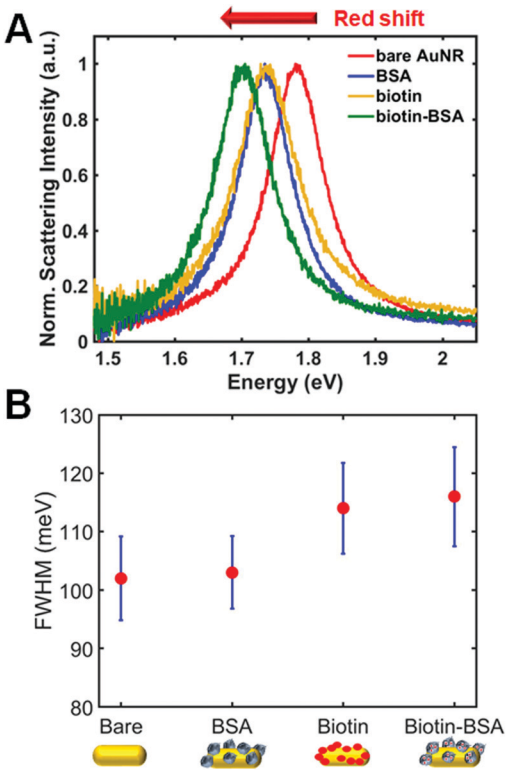

Fig. 5 (A) Single-particle scattering spectra according to different adsorbate molecules of BSA, BSA-biotin, and biotin. The scattering spectra are presented in eV. (B) Change in FWHM according to different adsorbate molecules of BSA, BSA-biotin, and biotin. In each case, 80 AuNRs were measured to compare the LSPR linewidth with statistics.

similar to that in the presence of BSA-biotin (Fig. 5B). Biotin molecules with a sulfur group were found to cause strong CID on single AuNRs, which has been demonstrated with thiol (–SH) molecules so far. We thus conclude that the increase in the LSPR linewidth in the cases of biotin and BSA-biotin results from the specific interactions of biotin with AuNRs through strong Au–sulfur binding. Further experimental data on the LSPR wavelength in the cases of bare AuNRs, BSA, biotin, and BSA-biotin are provided in Fig. S6 (ESI†).

There is also an important point that needs to be discussed in Fig. 4 and 5. Conventional LSPR biosensors are based on frequency shifts and are sensitive to both the surrounding medium and the adsorption of biomolecules. In our previous study, we demonstrated the effect of the refractive index of the surrounding medium on the LSPR linewidth of an AuNR. We found that the LSPR linewidth (or FWHM) remained almost constant when we increased the medium refractive index.[13,20] Therefore, we suggested that the CID of single AuNRs with thiol molecules can be used to develop label-free plasmonic sensors that have no sensitivity to the changes of the surrounding medium refractive index. However, it is also important to find real biological molecules that can cause CID and LSPR broadening for various biological studies. In this respect, it is important to notice that the current finding allows us to make a step forward toward the development of new LSPR biosensors based on CID (or the LSPR linewidth) with real biological

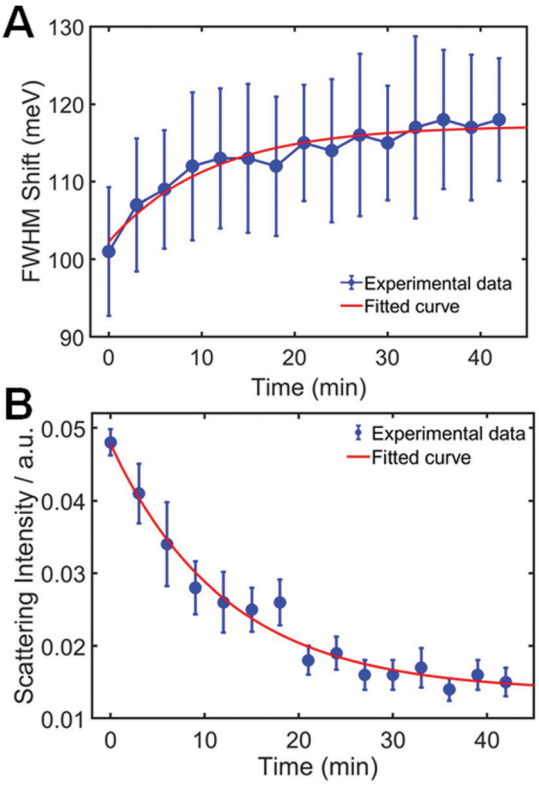

Fig. 6 The molecular binding effect on the LSPR linewidth of single AuNRs during a chemical reaction of BSA-biotin in real time. (A) The scattering spectra of the AuNRs deposited on a glass substrate were obtained as a function of time after adding BSA-biotin at a concentration of 10 μM in water. In this study, 3 AuNRs were measured to verify reproducibility under identical experimental conditions. (B) The corresponding change in the scattering intensity of AuNRs as a function of time with 3 min intervals.

molecules of biotin, which is widely used as a linker in many biological sensing studies.

Finally, we demonstrated that CID can be employed as a new approach for developing improved LSPR biosensors that can sense biotin molecules without interference from the medium dielectric constant. We investigated the molecular binding effect on the LSPR linewidth of single AuNRs during a chemical reaction of biotin in real time. We first measured the LSPR linewidth of single AuNRs in pure water before we added biotinylated BSA proteins. We then added those proteins (10 μM) in water onto the AuNRs fixed on a glass substrate and acquired single-particle scattering spectra as a function of time (3 min intervals). Fig. 6A shows the change of the LSPR linewidth of the AuNRs after the addition of the biotinylated BSA proteins. In this study, three single AuNRs were measured to verify reproducibility under identical experimental conditions. We observed that the FWHM shift was increased from 101 meV to 118 meV after we added the biotinylated BSA proteins in water. As supported in Fig. 4 and 5, the change of the LSPR linewidth in this study is ascribed to only the adsorption of biotin molecules on the AuNR surface. Fig. 6B shows the corresponding change in scattering intensity of AuNRs as a function of time. As shown in Fig. 6B, the scattering intensity decreased exponentially over time due to energy loss caused by CID, which is consistent with the result of the FWHM shift in Fig. 6A. Therefore, our findings make a step forward toward use of single AuNRs and CID for sensing biotin molecules having sulfur without interference from the medium refractive index in a variety of biological and chemical systems.

Conclusions

In summary, to better understand CID, we performed SEM-correlated DF scattering studies of single AuNR particles. We found that biotin with sulfur can lead to strong plasmon damping in single AuNRs. We chose biotin in this study to test as an alternative to thiol groups because it is widely used as a linker that can selectively bind to streptavidin in many biological sensing experiments. We further demonstrated the possibility of real-time detection of actual biological molecules, specifically, biotinylated BSA proteins, by means of CID of single AuNRs. Therefore, this study provides a deeper insight into how adsorbate molecules with sulfur affect CID and makes a step forward toward developing a CID-based LSPR biosensor to sense real biological molecules with sulfur or thiol groups using single AuNRs without interference from the medium dielectric constant. However, CID-based LSPR sensors can only be used to detect adsorbate molecules that strongly interact with the Au surfaces. Thus, further studies are necessary to find new functional groups that can induce strong CID in single AuNRs.

Conflicts of interest

There are no conflicts to declare.

Acknowledgements

This work was supported by a National Research Foundation of Korea (NRF) grant funded by the Korean government (MSIP) (no. 2018R1C1B3001154).

Notes and references

1 M. Pelton, M. Liu, S. Park, N. F. Scherer and P. Guyot-Sionnest, *Phys. Rev. B: Condens. Matter Mater. Phys.*, 2006, **73**, 155419.
2 A. Hoggard, L. y. Wang, L. Ma, Y. Fang, G. You, J. Olson, Z. Liu, W. S. Chang, P. M. Ajayan and S. Link, *ACS Nano*, 2013, **7**, 11209.
3 C. Sönnichsen, T. Franzl, T. Wilk, G. von Plessen, J. Feldmann, O. Wilson and P. Mulvaney, *Phys. Rev. Lett.*, 2002, **88**, 077402.
4 C. Novo, D. Gomez, J. Perez-Juste, Z. Zhang, H. Petrova, M. Reismann, P. Mulvaney and G. V. Hartland, *Phys. Chem. Chem. Phys.*, 2006, **8**, 3540–3546.
5 J. Olson, S. Dominguez-Medina, A. Hoggard, L.-Y. Wang, W.-S. Chang and S. Link, *Chem. Soc. Rev.*, 2015, **44**, 40–57.
6 M. Hu, C. Novo, A. Funston, H. Wang, H. Staleva, S. Zou, P. Mulvaney, Y. Xia and G. V. Hartland, *J. Mater. Chem.*, 2008, **18**, 1949–1960.

7 M. Hu, H. Petrova, A. R. Sekkinen, J. Chen, J. M. McLellan, Z.-Y. Li, M. Marquez, X. Li, Y. Xia and G. V. Hartland, *J. Phys. Chem. B*, 2006, **110**, 19923–19928.
8 X. Wang, Z. Zhang and G. V. Hartland, *J. Phys. Chem. B*, 2005, **109**, 20324–20330.
9 C. L. Nehl, N. K. Grady, G. P. Goodrich, F. Tam, N. J. Halas and J. H. Hafner, *Nano Lett.*, 2004, **4**, 2355–2359.
10 M. Hu, J. Chen, M. Marquez, Y. Xia and G. V. Hartland, *J. Phys. Chem. C*, 2007, **111**, 12558–12565.
11 J. W. Ha, W. Sun, A. S. Stender and N. Fang, *J. Phys. Chem. C*, 2012, **116**, 2766–2771.
12 P. Zijlstra, P. M. R. Paulo, K. Yu, Q. H. Xu and M. Orrit, *Angew. Chem., Int. Ed.*, 2012, **51**, 8352.
13 J. W. Ha, *Chem. Phys. Lett.*, 2017, **676**, 65–69.
14 B. Foerster, A. Joplin, K. Kaefer, S. Celiksoy, S. Link and C. Sönnichsen, *ACS Nano*, 2017, **11**, 2886–2893.
15 Y. Zhang, S. He, W. Guo, Y. Hu, J. Huang, J. R. Mulcahy and W. D. Wei, *Chem. Rev.*, 2018, **118**, 2927–2954.
16 K. Wu, J. Chen, J. R. McBride and T. Lian, *Science*, 2015, **349**, 632–635.
17 M. L. Brongersma, N. J. Halas and P. Nordlander, *Nat. Nanotechnol.*, 2015, **10**, 25.
18 P. Christopher and M. Moskovits, *Annu. Rev. Phys. Chem.*, 2017, **68**, 379–398.
19 A. O. Govorov, H. Zhang and Y. K. Gun'ko, *J. Phys. Chem. C*, 2013, **117**, 16616–16631.
20 S. W. Moon, P. V. Tsalu and J. W. Ha, *Phys. Chem. Chem. Phys.*, 2018, **20**, 22197–22202.

